Smart Solutions in Smart Spaces

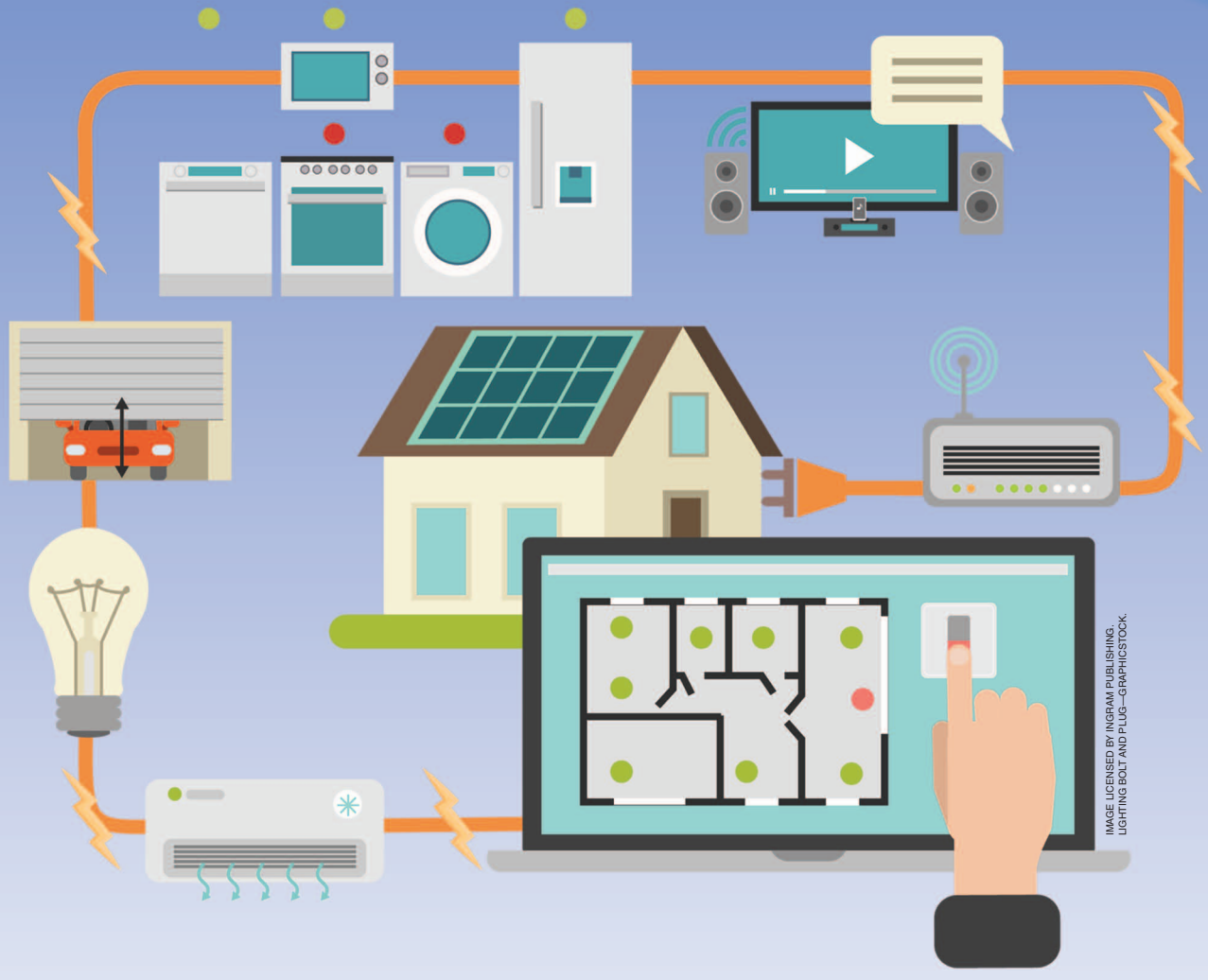

IMAGE LICENSED BY INGRAM PUBLISHING. LIGHTNING BOLT AND PLUG—GRAPHICSTOCK.

Alessandra Costanzo and Diego Masotti

Alessandra Costanzo (alessandra.costanzo@unibo.it) and Diego Masotti (diego.masotti@unibo.it) are with the Department of Electrical, Electronic, and Information Engineering (Guglielmo Marconi), Alma Mater Studiorum, University of Bologna, Italy.

Digital Object Identifier 10.1109/MMM.2016.2525119
Date of publication: 7 April 2016

In the very near future, an almost unlimited number of monitoring applications—structural health, logistic, security, health care, and agriculture to name only a few—will require large-scale deployment of cooperative wireless microsystems with sensing capabilities, moving us closer to the effective realization of the paradigm of the Internet of Things (IoT).

The main open challenge here lies in the reliability of maintenance-free, long-lived devices, especially from the standpoint of energy sustainability. Such systems are required to power themselves by harvesting energy from the ambient sphere, thus eliminating the need for batteries. To minimize energy requirements, wake-up radios able to be activated by signals as low as –50 dBm are already available [1]. Many foresee RF/microwave energy sources as one of the best candidates to comply with energy autonomy, either because they are widely distributed in humanized environments or because they can be efficiently provided on demand.

These two different ways of providing RF energy can be referred to as *energy harvesting* (*EH*) and *wireless power transmission* (*WPT*), respectively. In either case, careful design of the RF power transfer link, consisting of nonlinear subsystems and radiating elements, is required to assure that their characteristics are carefully optimized for each particular scenario.

Intensive industrial and academic activities have been devoted to this field: several techniques and circuit solutions have been concurrently proposed and tested to ensure sufficient and non-intermittent wireless power transfer with the lowest possible density. In this way, it is possible to simultaneously achieve maximum transfer efficiency and minimum electromagnetic (EM) interference and pollution.

Typical frequencies adopted for these purposes are in the ultrahigh-frequency (UHF) and super high-frequency bands—around 400–800 MHz for terrestrial television signals and around 900, 1,800, 2,400, and 5,800 MHz for different wireless standards: since the geometric area to be covered is usually of the order of few meters, the devices to be powered are in the far-field region of their known or unknown RF/microwave sources.

This article reviews some recent promising circuit and antenna solutions and discusses reliable subsystems adopted for receiving and transmitting along with their associated radiating elements, with a focus on minimizing the power budget enabling device operations.

Block Representation of a Far-Field Power Transfer System

Figure 1 shows a block chain representation of an entire far-field wireless power system, from the transmitter dc bias to the receiver dc output: it consists of a power source connected to a transmitting antenna system, the radio channel, and a receiving antenna system connected to a rectifier circuit whose dc output is managed by a dc-to-dc converter that provides the energy to the batteryless device [2], [3]. The significant power quantities to be monitored at each subsystem connecting port are also outlined in Figure 1.

Exact knowledge of these quantities can be used to compute overall system efficiency as a product of the following ratios:

$$\eta_{TOT} = \eta_{BIAS-RF} \cdot \eta_{RF-RF} \cdot \eta_{RF-DC} \cdot \eta_{DC-DC} = \frac{P_{TX}}{P_{BIAS}} \cdot \frac{P_{RX}}{P_{TX}} \cdot \frac{P_{DC}}{P_{RX}} \cdot \frac{P_{ST}}{P_{DC}}, \quad (1)$$

where P_{BIAS} is the dc power required at the transmitter side, P_{TX} is the RF power available at the transmitting antenna input port, P_{RX} is the RF power received by the antenna, P_{DC} is the rectifier output power, and P_{ST} is the dc-to-dc converter output power. Of course, all these quantities are dependent on the operating frequencies and on the power densities involved, due to the nonlinear nature of the link building blocks.

The first factor is the dc-to-RF conversion efficiency of the power source. The second one accounts for the transmitting and receiving antennas performances and the radio channel multipath and fading effects, which are linear but frequency-dependent and determine the geometric range that can be covered by the RF source. A rigorous circuit-equivalent model formulation to accurately evaluate this contribution can be derived by EM theory [4]. The third factor is the RF-to-dc conversion efficiency of the rectifier. The last factor is the dc-to-dc conversion efficiency of a power management unit that is optimized to dynamically track the rectifier optimum load. Because the entire WPT system consists of a connection of nonlinear circuits, its behavior is strongly dependent on the power levels involved—on the RF sources' waveforms and operating frequencies—and can be precisely quantified only if such blocks' behaviors are exactly known.

Furthermore, (1) can be exactly evaluated only in case of intentional WPT sources; it is not possible in EH scenarios where ambient available RF sources are exploited. For energy scavenging purposes, the transmitter side is not under control, but the available RF sources distributed in the ambient are used. Thus, only the RF behavior of the rectifier

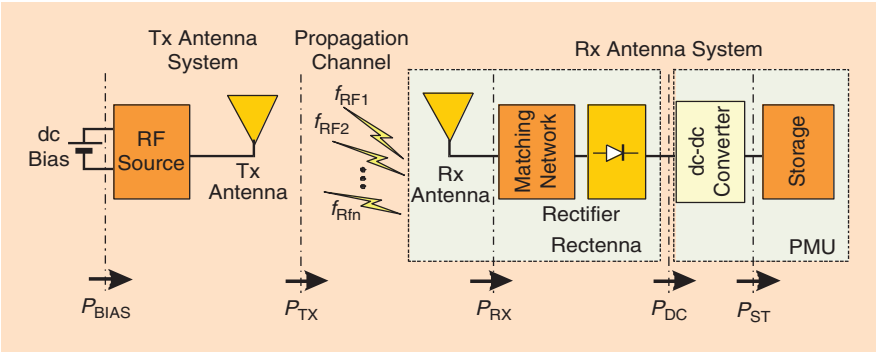

Figure 1. *The building blocks of a far-field wireless power transfer system, along with the power quantities involved. Tx: transmitter; Rx: receiver.*

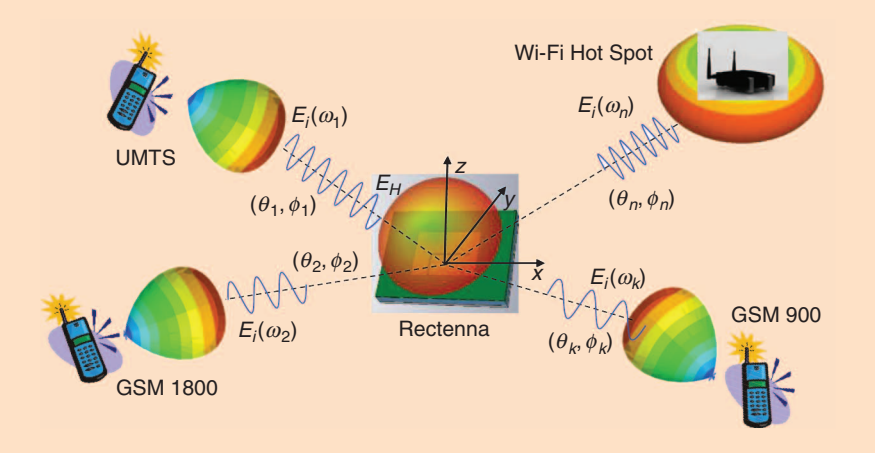

Figure 2. *An EH scenario with multiple, randomly distributed RF sources [3]. UMTS: Universal Mobile Telecommunications System; GSM: Global System for Mobile Communications.*

and the baseband operation of the power-management unit (PMU) can be optimized using a realistic estimation of the available power densities, such as those provided in [5]–[9].

Wireless Powering from Ambient Energy and On Demand

Two different scenarios for wireless powering are schematically depicted in Figures 2 and 3: these can be considered *wireless powering from ambient RF energy* (i.e., EH) and *wireless powering on demand* (i.e., WPT). The EH scenario in Figure 2 shows devices, randomly present in the environment, scavenging energy from RF sources at different operating frequencies based on television, Wi-Fi, and cell phone standards. In this case, the available energy is ambient-dependent and highly time-variable. Furthermore, the transmitter side performance (such as the dc-to-RF conversion efficiency), the RF output power, and the antenna radiation behavior are not available and can only be roughly estimated. The same is true for knowledge of the radio channel.

Thus, the RF receiver side—commonly referred as the *rectenna* (for "rectifying antenna")—must be designed to comply with these uncertainties, and the antennas should feature broadband or multiband behaviors to cover all the wireless standards available in the ambient sphere, with circular or dual polarization to ensure signal reception in any link conditions. Because the ultimate goal is to scavenge all RF sources at the same time and at any possible frequency, polarization, angle of arrival, and power intensity, it is apparent that the design of such harvesting systems is a very demanding task. Furthermore, it has been proven [5]–[9] that the available ambient RF power density is usually very low (ranging from a few nanowatts to a few microwatts per square centimeter), so highly efficient (resonant) antennas as well as carefully optimized rectifiers are needed. Finally, because such radiating systems need be integrated in low-weighted miniaturized devices, a compromise between performance and optimum size is necessary.

Figure 3 shows the schematic for a WPT scenario with dedicated, known RF sources. In this configuration, the receiving system design takes advantage of the knowledge of the RF frequencies, the direction of arrival, and the polarization of the incident power. For example, dedicated RF sources, ready to provide the necessary (low) energy when requested [3], may be installed. This case is similar to the powering of passive RF identification (RFID) tags. In such situations,

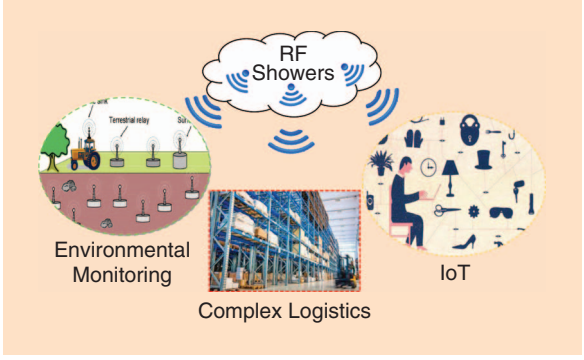

Figure 3. *A WPT scenario with dedicated, known RF sources.*

a different design approach from the previous one should be followed because any WPT system building block can be deterministically predicted and the available power densities at the batteryless device's location can be more accurately evaluated. Directive, single-band, resonant antennas having polarizations coherent with those of the transmitting side can be used, and the overall system efficiency can thus be precisely maximized. Later in the article, we will show that, in such situations, power density minimization can be obtained by exploiting optimized transmitted signal waveforms and smart beaming strategies to focus the energy on demand.

As a result, adopting dedicated RF sources is being touted as the most promising choice for the effective implementation of IoT scenarios: on the one hand, they allow a precise knowledge of the energy availability, thus ensuring the safe range for device powering; and, on the other hand, such energy can be focused and provided in such a way that the receiver-side efficiency is enhanced.

The design features, the degrees of freedom, and the available information for wireless powering from ambient energy and for intentional wireless powering are summarized in Tables 1 and 2, respectively.

Table 1. EH system characteristics.

Wireless Powering from Ambient Energy		
Transmitter side	Power generator	• Not controllable • Multitone
	dc-to-RF efficiency	• Cannot be optimized
	Antenna specifications	• Directivity unknown • Polarization and position unknown • Multiband sources
Radio channel	RF-to-RF efficiency	• Unknown • Worst case (statistical) estimate
Receiver side	Rectifier	Design as a compromise for a broad range of power densities and frequencies
	RF-to-dc efficiency	Can be optimized
	Antenna specifications	• Nondirective • Circularly or dual polarized • Multiband resonant

Table 2. Intentional WPT system characteristics.

Wireless Powering on Demand		
Transmitter side	Power generator	• High efficiency power amplifier • Optimized signal waveforms (multisine, ultrawide-band, chaotic signals)
	dc-to-RF efficiency	• Can be optimized
	Antenna specifications	• Directive • Defined polarization and position • Smart beaming is possible
Radio channel	RF-to-RF efficiency	• Known • Optimized
Receiver side	Rectifier	Design for specific power densities and RF frequencies, multistage topology
	RF-to-dc efficiency	Can be optimized
	Antenna specifications	• Directive • Defined polarization and position • Single-band

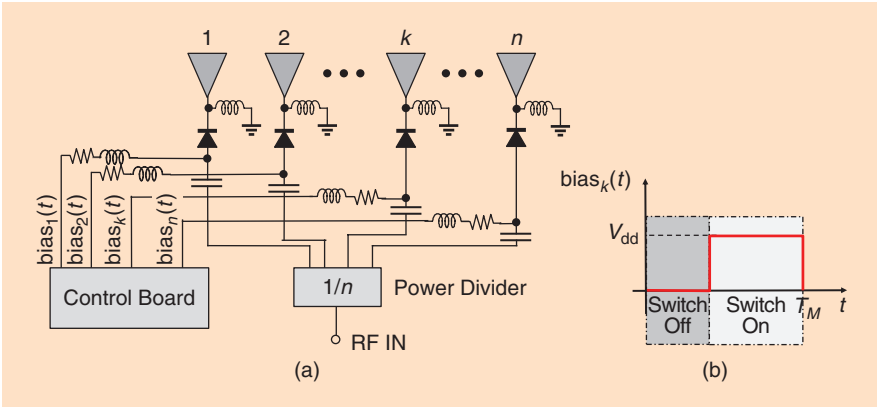

Figure 4. *(a) A schematic representation of a linear TMA with n radiating elements and (b) the generic k-th element rectangular pulse for k-th antenna control.*

Power Transmission Optimization Challenges

In order to enable energy autonomy for a plethora of low-power wireless nodes located in ad hoc positions, the focus for the power transmission subsystem is not only on maximizing the power source dc-to-RF efficiency, but also on maximizing the range to be covered with the minimum power density in the ambient sphere. Indeed smart power sorting can assist in keeping the lowest possible power density in the ambient sphere, thus minimizing interference and EM pollution. We show that, once the transmitter efficiency maximization is ensured by means of the vast number of techniques available from the power amplifier design [10]–[13], the WPT transmitter's capabilities can be augmented by a suitable real-time beaming technique to focus the transmitting antenna system in the direction of the devices to be powered.

Furthermore, the adoption of optimized multitone transmitted waveforms can enhance the receiver range by boosting the rectifier's operation, especially at low-input RF powers, thus increasing its RF-to-dc conversion efficiency. These two aspects are considered to be strategic ones for scenarios where the locations of batteryless devices can be precisely determined so that the radio channel is known and the RF-to-RF efficiency can be exploited to minimize the power density without compromising device operations.

Power Beaming

At the transmitter side, smart power beaming can be of strategic importance in view of energy-aware WPT systems. For this purpose, time-modulated arrays (TMAs) have been recently proposed in [14] for an energy-efficient and precise WPT procedure. The schematic representation of an n-port radiating system of this kind is shown in Figure 4(a): the nonlinear RF switches, connected at each antenna port, are driven by periodical sequences of rectangular pulses ($\text{bias}_k(t)$, $k = 1,2,\ldots, n$) of period $T_M = 1/f_M$ and amplitude V_{dd}. Figure 4(b) illustrates the signal at the generic k-th switch.

In this way, the radiation pattern at the RF carrier (f_0) to be radiated can be dynamically synthesized by modifying the on/off ratio of the switch's excitation period [15] and the switch-on time instant [16], [17], thus creating an almost unlimited number of array-control sequences. The control sequence of a 16-dipole array, reproducing a Dolph-Chebyshev excitation for side-lobe level reduction, is provided as an example in Figure 5(a); Figure 5(b) shows the corresponding radiation pattern at the fundamental frequency, with

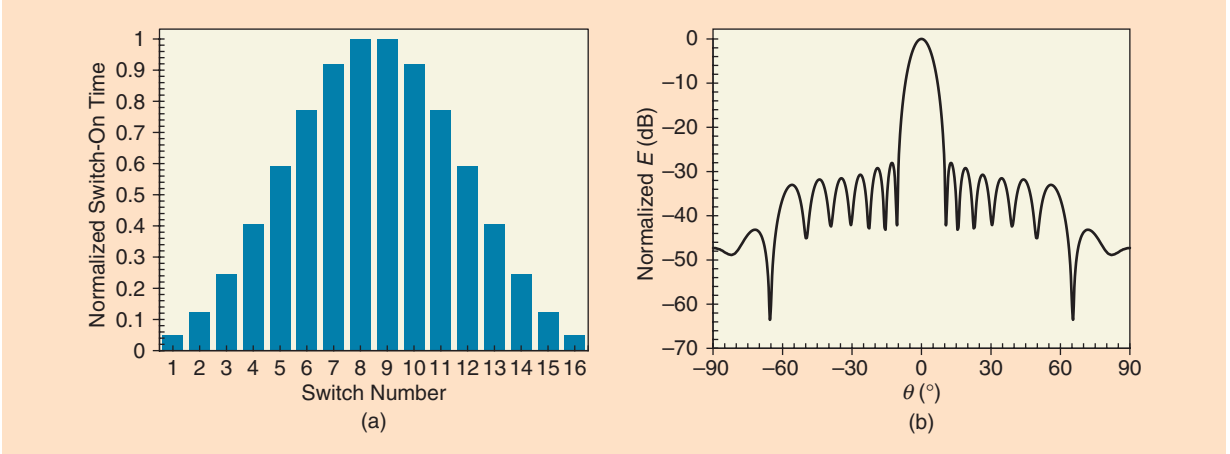

Figure 5. *(a) The normalized switch-on time of the 16 nonlinear switches of a dipole array, reproducing a Dolph-Chebyshev pattern for side-lobe level control; and (b) the corresponding radiation pattern at the fundamental frequency with a side-lobe level equal to –30 dB.*

a side-lobe level of –30 dB. Note that TMAs also allow a simpler architecture with respect to other beam forming solutions, such as phased-arrays [18] or retrodirective arrays [19]: in fact, they do not need phase shifters to create the proper phase condition at the antenna ports.

Due to the superposition of the periodic switch control sequences (at frequency f_M) with the RF carrier frequency f_0, TMAs are able to radiate not only at the fundamental carrier (f_0, $h = 0$) but also at the sideband harmonics ($f_0 + hf_M$, $h \neq 0$). This property has been exploited in [14] for a smart two-step WPT procedure via TMAs: first, a two-element time-modulated subarray is used for localization of tagged sensors to be energized; then, the entire TMA provides the power to the detected tags.

The TMA adopted in [14] for the smart WPT activity is the uniform 16-monopole planar array shown in Figure 6: it operates at f_0 = 2.45 GHz, and is realized on a Taconic RF60A substrate (ε_r = 6.15, thickness = 0.635 mm). The spacing between the elements is the standard $\lambda/2$ distance. As switching elements, microwave Schottky diodes (Skyworks SMS7630-079) are used, driven by periodic sequences having a modulation frequency of f_M = 25 kHz.

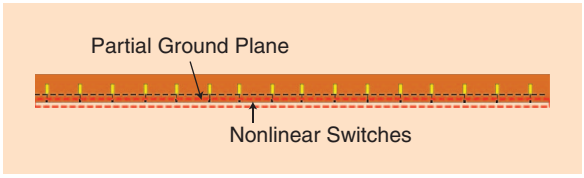

Figure 6. *The layout of the uniform 16-monopole linear TMA in [14].*

Localization of the Tags

In the first step of the WPT procedure, the TMA is used to detect n tagged sensors. At this stage, the 14 peripheral switches are left open, and the sole dual-inner-element subarray is operating. By piloting the two switches in the way indicated in Figure 7(a) [20], it is possible to obtain the fundamental radiation pattern at f_0 with the sum (Σ) shape, while at the first harmonics, $f_0 \pm f_M$, the shape of the difference (Δ) is reproduced. By modifying the excitation duty cycle (parameter δ), it is also possible to scan the Δ pattern in the way indicated in Figure 7(b): with the two inner monopoles of the array shown in Figure 6, a scanning region of about ±60° is achieved.

After a standard RFID reading operation to acquire the tags' IDs, the sharpness of the negative peaks of the steered Δ patterns allows high resolution in the localization phase; this fact can be exploited by means of a suitable combination of the received signal-strength indicators backscattered by the tags, using both the Σ and Δ patterns, to build the maximum power ratio (MPR) [21]:

$$\mathrm{MPR}(\theta) = \sum_{\mathrm{RSSI}}^{\mathrm{dB}}(\theta) - \Delta_{\mathrm{RSSI}}^{\mathrm{dB}}(\theta). \qquad (2)$$

The combination of the figure of merit (2) with the scanning capability has proven its effectiveness in indoor localization, with resolution up to few centimeters at 2.45 GHz [21]: the number of steps to discretize the scanning window [21] is now realized by the same number of control parameter δ variations, providing the associated switch's control sequences of the kind reported in Figure 7(a).

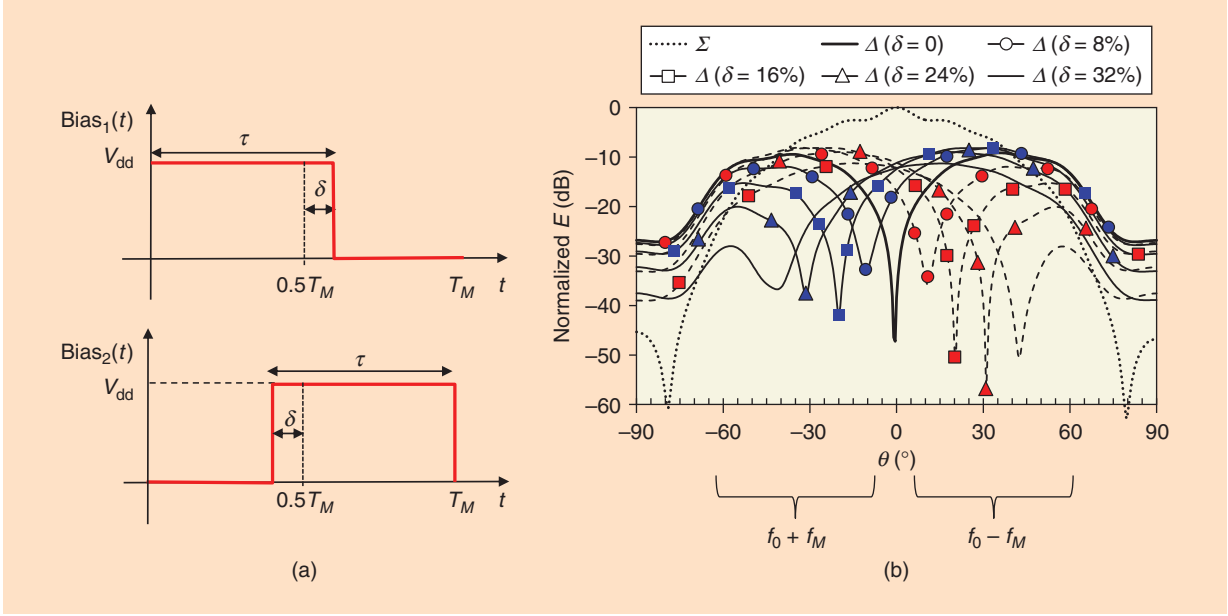

Figure 7. *(a) The control patterns of the two inner-array element switches, providing Σ and Δ patterns; and (b) the corresponding simulated Σ and Δ radiation patterns for different δ values [14].*

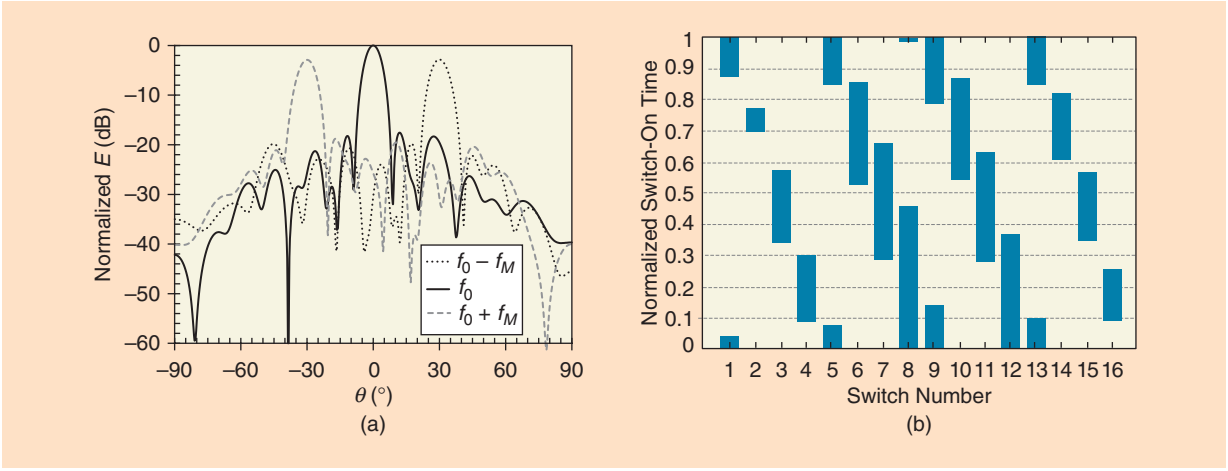

Figure 8. *(a) The fundamental and the first sidebands' radiation patterns of the 16-element array for the simultaneous power transfer in $\theta = -30°, 0°, 30°$ directions [14]; and (b) the corresponding control sequence showing the normalized switch-on time of the 16 nonlinear switches [16].*

At the end of the scanning activity, a vector with the n values of θ corresponding to the peaks of the received MPRs (θ_{peak}) is recorded.

Power Transfer to the Tags

Once the tags' positions have been retrieved, the whole 16-element array of Figure 6 is used, applying the control sequences to all the switches—thus, providing the desired power-beaming behavior. One has to imagine the TMA switches' controller to have been preloaded with the list of control sequences capable of realizing different radiation patterns. In the case given here, a possible decision rule during the WPT activity could be to split the scanning region ($\theta \in [-60°$ $60°]$) into sectors of amplitude equal to the half-power beam width (HPBW) (7° in this case): for each θ_{peak} falling in the sector centered around θ_{HPBW}, the TMA controller loads the control sequence pointing the first harmonic to the θ_{HPBW} direction.

For instance, in case of a θ_{peak} falling in the sector centered around $\theta_{HPBW} = 0°$, the fixed fundamental harmonic beam can provide the energy to the corresponding sensor, while the two sideband harmonics ($h = \pm 1$) can be used to simultaneously energize another couple of symmetrically placed tags. Figure 8(a) describes a possible solution in case of three detected tags falling inside the sectors $\theta_{HPBW} = -30°, 0°, 30°$: the multibeam performance is obtained by driving the switches with the control sequence shown in Figure 8(b) [16], which represents the result of an optimization procedure with specifications on the sideband beams' pointing directions, as well as on their amplitudes. In this way, the higher harmonic power peaks are only a few decibels (~3 dB) below the fundamental one.

Optimizing the Transmitted Signal Waveform

Recent studies [22]–[24] have demonstrated that rectifier circuits designed to manage low RF input power—of the order of –20 dBm or lower—improve their rectification performance when driven by multisine waveforms with a high peak-to-average power ratio (PAPR), in place of continuous-wave (CW) signals having the same average power. In this way, the efficiency limitations due to the diode turn-on at low input powers can be overcome. It must be noted that, to be effective, the multisine waveforms of the high-PAPR signals need be carefully designed to ensure the proper phase relationships to realize higher dc rectifier output power. In the experiment of [23], voltage spikes occur when the tones are aligned in phase, as shown in Figure 9; this increases the efficiencies at low RF powers (typically less than 0 dBm) at the expense of bandwidth, whereas a decreased efficiency at higher powers (typically greater than 0 dBm) is observed.

Figure 10(a) and (b) [23] shows the rectification behavior in the case of a single-frequency CW excitation and of a high-PAPR signal with the same power density. Fully exploiting this promising technique requires that the entire RF radio link be controlled to ensure the proper phase relationships.

Different time-domain waveforms—such as orthogonal frequency-division multiplexing (OFDM), white noise, and chaotic waveforms—have been tested in [25] to assist the rectifier's operations from the transmitter side, at received power levels up to 0 dBm. As illustrated in Figure 11, these experiments confirmed that, due to the intrinsically high PAPR of such modulation formats, the efficiency is boosted to a quantity better than 15% for RF input power lower than –5 dBm.

However, for a given diode selection, this technique is adoptable only over a defined low-power range (e.g., between –20 and –10 dBm for a rectifier adopting the Avago HSMS-2865 diode [24]); this is numerically and experimentally demonstrated in [26], although different modulation formats with respect to [25] are used. It is noteworthy that the upper limit is defined by the

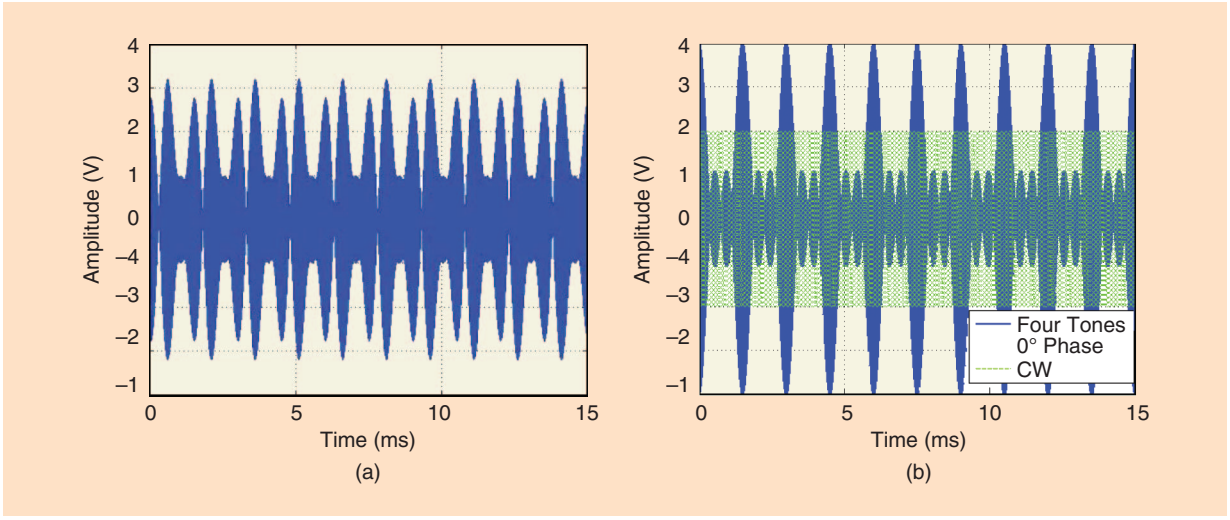

Figure 9. *Time-domain waveforms: (a) a four-tone multisine with a random phase arrangement and (b) a four-tone with 0° phase arrangement, overlapped with a CW having the same average power [23].*

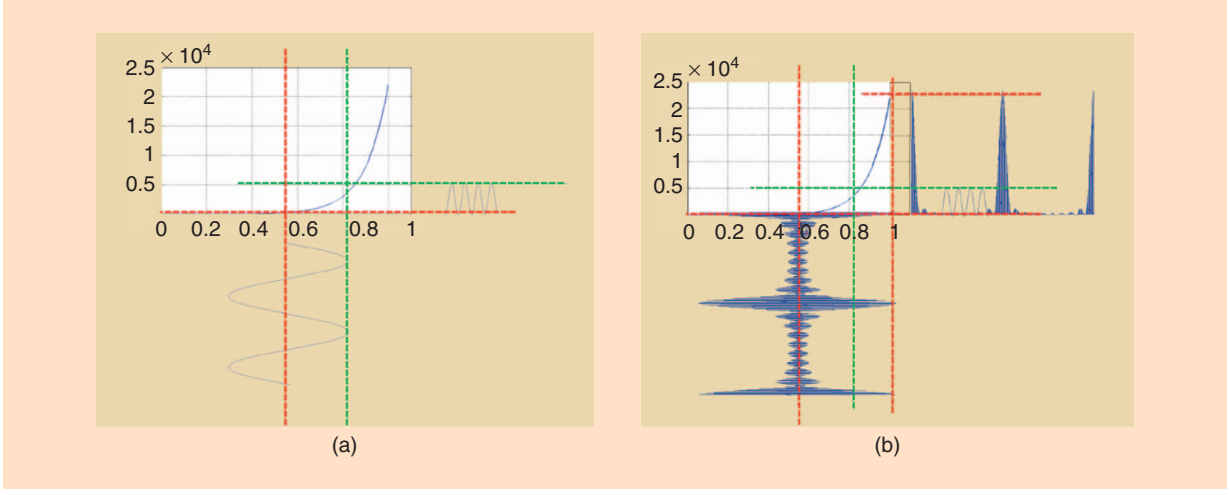

Figure 10. *The rectification of (a) a sinusoidal signal and (b) a high-PAPR multisine signal (with currents in μA and voltages in V) [23].*

specific diode adopted and is related to its voltage breakdown.

Figure 12 compares measured rectifier conversion efficiency at power levels spanning 0–10 dBm for a CW and quadrature phase-shift keying (QPSK)-modulated signals with increasing bit rate. In this case, efficiency degradation is observed all over the input power range, and it increases with the bit rate due to the demand of a larger bandwidth. Again, the specific power boundaries vary with the rectifier topology and the diode-like devices adopted.

The Receiver Side: Maximizing the Received Power

The low amount of available RF power in real environments [5]–[9] has led to hybrid solutions for energy harvesters, exploiting the coexistence of different energy sources besides the RF ones, as depicted in Figure 13.

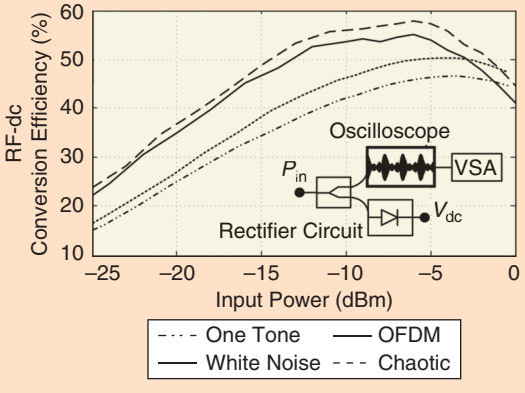

Figure 11. *The RF-dc conversion efficiency of the rectifier circuit versus total input power for different test signals [25].*

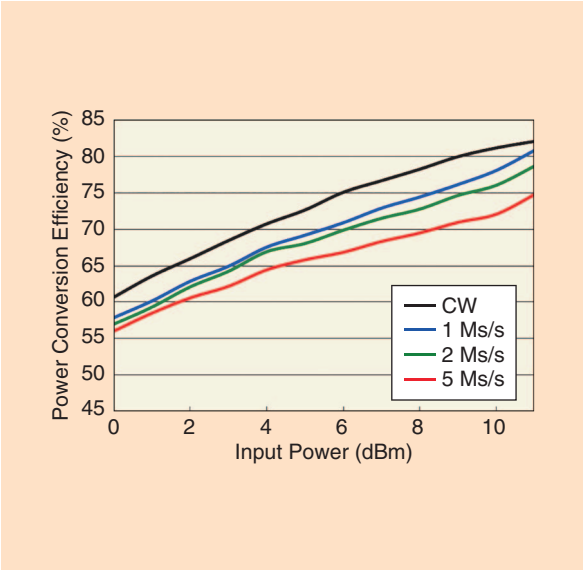

Figure 12. *The measured conversion efficiency of QPSK-modulated signals [26].*

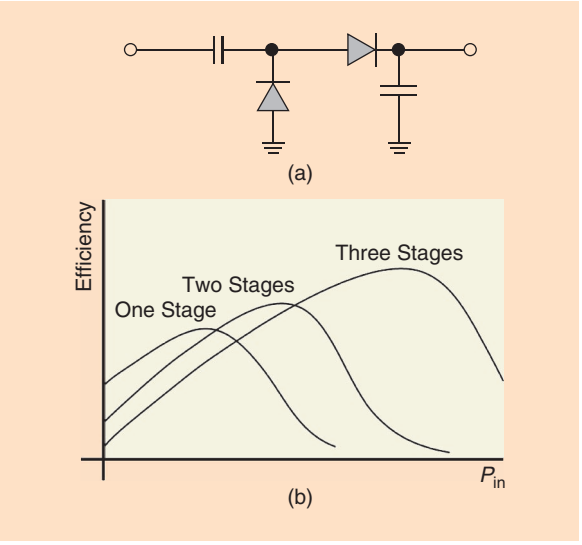

Figure 14. *(a) A single-stage full-wave rectifier topology and (b) RF-to-dc efficiency behavior versus input RF power for different numbers of rectifying stages [33].*

Vibrational energy is the additional source proposed in [28], while the planar rectenna area is exploited to host a photovoltaic cell in [29]. In [30], flexible fabrics are shown to be a suitable support for multiple scavenging transducers deploying RF, solar, and thermal sources. In all these solutions, the cooperative action of different sources demonstrates an improvement in the total harvester conversion efficiency.

In practical EH applications, the final user of the power rectified by the rectenna is a device operating discontinuously, e.g., a sensor that needs to be activated during very short time intervals and for a few times per day. As a consequence, rectennas must include an intermediate energy buffer (or PMU) able to manage the variable workload conditions. Well-established solutions consist of dc-to-dc switching converters capable of dynamically tracking the maximum power point (MPP) condition: a rectified voltage of about one half the open-circuit one has been shown to be close to the optimum condition for any frequency and power level [31], [32].

The proper choice of the rectifier topology can significantly enhance the RF-to-dc conversion efficiency, as well. For the extremely low RF power budgets involved, the use of two Schottky diodes arranged in the single-stage full-wave rectifier (or voltage doubler) topology shown in Figure 14(a) has been demonstrated to provide the most convenient choice, because of the reduced diode losses [33]. An increase in the number of stages can be justified only in different scenarios, such as in RFID tag applications, that involve higher power levels, as shown in Figure 14(b).

A recent study described in [34] has demonstrated a significant advantage in using backward tunnel diodes instead of traditional Schottky ones. The tunnel diodes' operating principle is based on the quantum mechanical tunneling effect rather than on the thermionic emission effect of the Schottky diodes. This has been proven to be sufficient to significantly increase the RF-to-dc conversion efficiency of

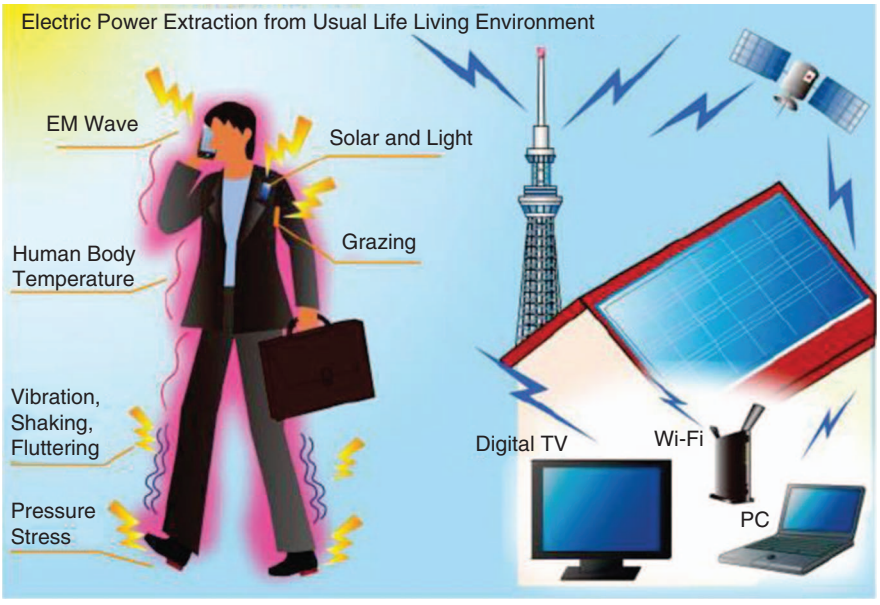

Figure 13. *Available environmental sources [27].*

a half-wave rectifier (single diode) prototype: measurements of RF-to-dc conversion efficiency at –40 dBm/2.4 GHz show that the backward diode outperforms the HSMS-285B Schottky diode by a factor of 10.5 and the Skyworks SMS 7630 by a factor of 5.5 [34]. However, one limiting factor for exploiting these diodes is the very high real-part impedance observed in the UHF band (hundreds of Ω), which is not easily matched.

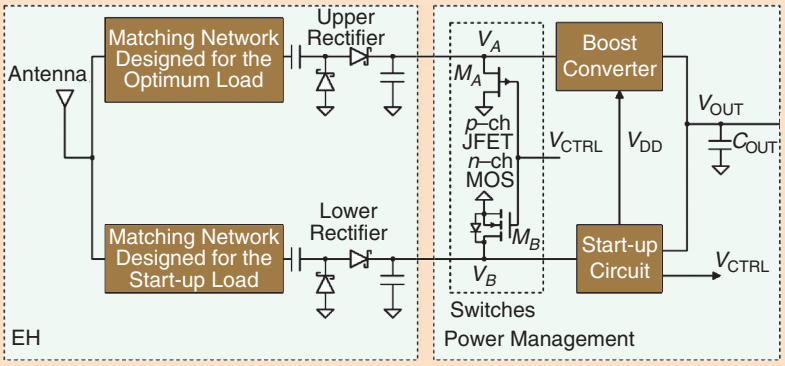

Figure 15. *A block diagram of the two-branch rectifier proposed in [35].*

Still, an energy-autonomous subsystem is an issue when ultralow-power densities are concerned. In the following sections, we point out some of the recent novelties in rectenna designs that are paving the way toward the exploitation of RF scavengers in real scenarios.

Dual-Mode Rectifiers

The main restriction on exploiting rectennas, even if operating in MPP condition, consists of the low values of the rectified voltages they typically provide—lower than the threshold voltage of diodes and transistors, and thus not able to wake up the PMU.

A possible solution to this problem is proposed in [35], where a novel rectifier design approach addresses the problem at RF, instead of at the baseband. As shown in Figure 15, the antenna is loaded by a parallel connection of two matching network/rectifier assemblies: the lower one is optimized to operate when extremely low powers are involved during the start up, and its goal is to autonomously obtain the needed dc voltage to start up the PMU, even if this is obtained at reduced RF-to-dc conversion efficiencies; the upper branch operates in maximum conversion efficiency condition soon after the minimum dc voltage to activate the PMU is reached.

The complex design of the two-way rectifier can be accomplished by exploiting the highly different load conditions offered by the two operating regions, as explained in Figure 16(a) referring to a standard rectenna: an almost open-circuit load pertains to the start-up condition, in conjunction with the desired high dc voltage; a lower resistive load characterizes the second branch, together with higher conversion efficiency. In this way, two mutually exclusive and alternatively matched paths represent the antenna load in the two operating conditions (the upper and lower rectifiers illustrated in Figure 15). It is noteworthy that, during the start-up step, the main goal is to reach the dc voltage needed to autonomously enable the dc-dc converter operation, accepting poor conversion efficiency. Once this goal is reached, the start-up branch is strongly

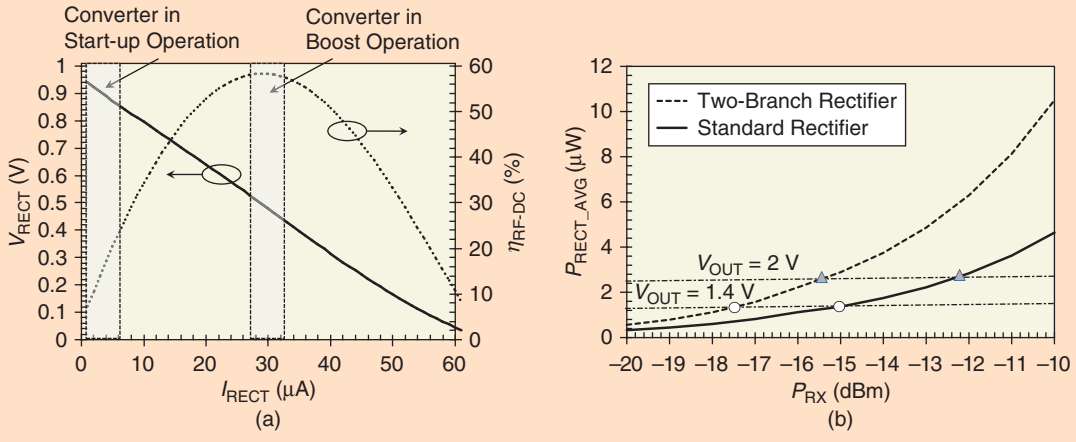

Figure 16. *(a) Optimized rectifier efficiency and output dc voltage as a function of the load current consumption (for P_{RX} = 25 μW) and (b) average output dc power P_{RECT_AVG} versus input power P_{RX} in the case of a dual-branch and of a conventional single-branch rectifier (both loaded with the start-up circuit) [35].*

The low amount of available RF power in real environments has led to hybrid solutions for energy harvesters, exploiting the coexistence of different energy sources besides the RF ones.

mismatched to the antenna with a reflection coefficient higher than –4 dB, which is now loaded by the upper rectifier [35]. In this way, the lower branch drains only a negligible amount of RF power.

Figure 16(b) demonstrates the advantage of this topology, by comparing the measured average powers rectified by a standard rectifier and by the new two-branch rectifier, as a function of the incoming RF power level. In practice, this novel solution allows a prescribed voltage to be achieved with half the available RF power needed in the standard case.

Resistance Compression Networks

Typically, a rectifying circuit is designed to provide the maximum RF-to-dc efficiency for a given fixed load and signal level. As noted previously, this represents a limitation with respect to the actual rectifier operating conditions for two reasons: 1) the nonlinear behavior of the rectifier is strongly dependent on the RF available power provided by the receiving antenna, and 2) the actual rectifier load is a dc-to-dc converter, as depicted in Figure 1, emulating a variable load impedance—changing, for instance, with the charging level of the storage capacitor. For these reasons, the design of the rectenna matching network becomes a demanding task, due to the highly variable impedance offered by the rectifier.

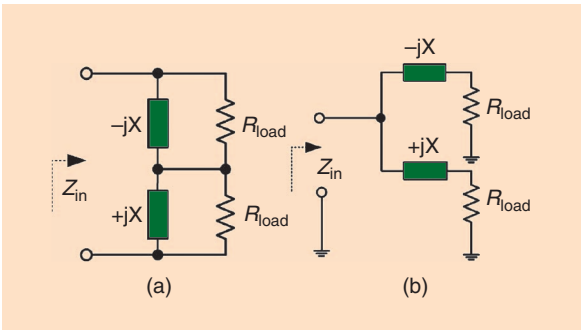

Figure 17. *The structure of two basic resistance compression networks [36]; formulas for (a) and (b) are provided in the text discussion.*

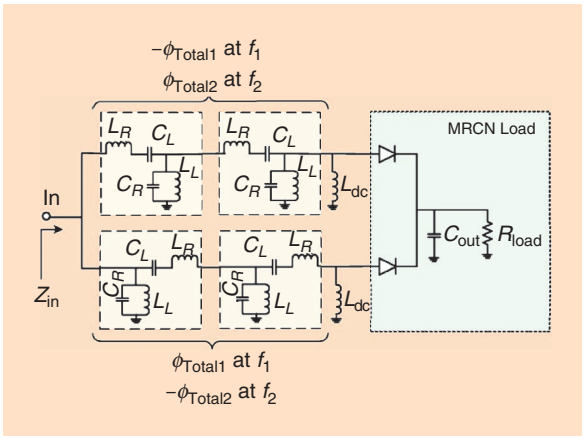

Figure 18. *The schematic of a rectifier circuit with a multiband resistance compression network (MRCN) [37].*

An interesting solution to this problem is proposed in [36] by means of a new class of matching networks, called *resistance compression networks*, that greatly reduce the variation of the effective resistance seen at their input port as loading impedance changes. The simple linear circuits shown in Figure 17 represent two (dual) solutions of these kinds of networks, exploiting reactive branches: here, R_{load} represents the real load varying across a wide range, whereas X is a specified reactance offered by the two branches, with identical amplitudes and opposite phases, at the designed operating frequency.

The relationships between the input resistance (R_{in}) and the load (R_{load}) is given by the simple formulas

$$R_{in-a} = \frac{2R_{load}}{1+\left(\frac{X}{R_{load}}\right)^2}$$
$$R_{in-b} = \frac{X^2}{2R_{load}}\left[1+\left(\frac{R_{load}}{X}\right)^2\right], \quad (3)$$

where the subscripts a and b stand for the cases of Figure 17(a) and (b), respectively, and the compression of the load resistances is around a center value equal to X.

A practical limitation in the use of compression networks in EH applications (see Table 1) is the need for wideband or multiband solutions for a complete coverage of the available wireless standards (as discussed in the following section): the amplitude and phase conditions on the reactance X should be valid at all the rectenna operating frequencies.

To overcome this problem, a dual-band compression network, of the kind shown in Figure 17(b), operating at 915 MHz and 2.45 GHz is proposed and realized in [37]. The topology illustrated in Figure 18 shows the adopted solution, providing the required opposite phase condition by using networks with reversed input and output ports in the two branches. Figure 19 demonstrates the comparison between the dual-band rectifier of Figure 18 and a standard rectifier, optimized at the two frequency bands: the advantage of the new solution with respect to the standard one, both in terms of load resistance [Figure 19(a) and (b)] and input power variations [Figure 19(c) and (d)], is evident.

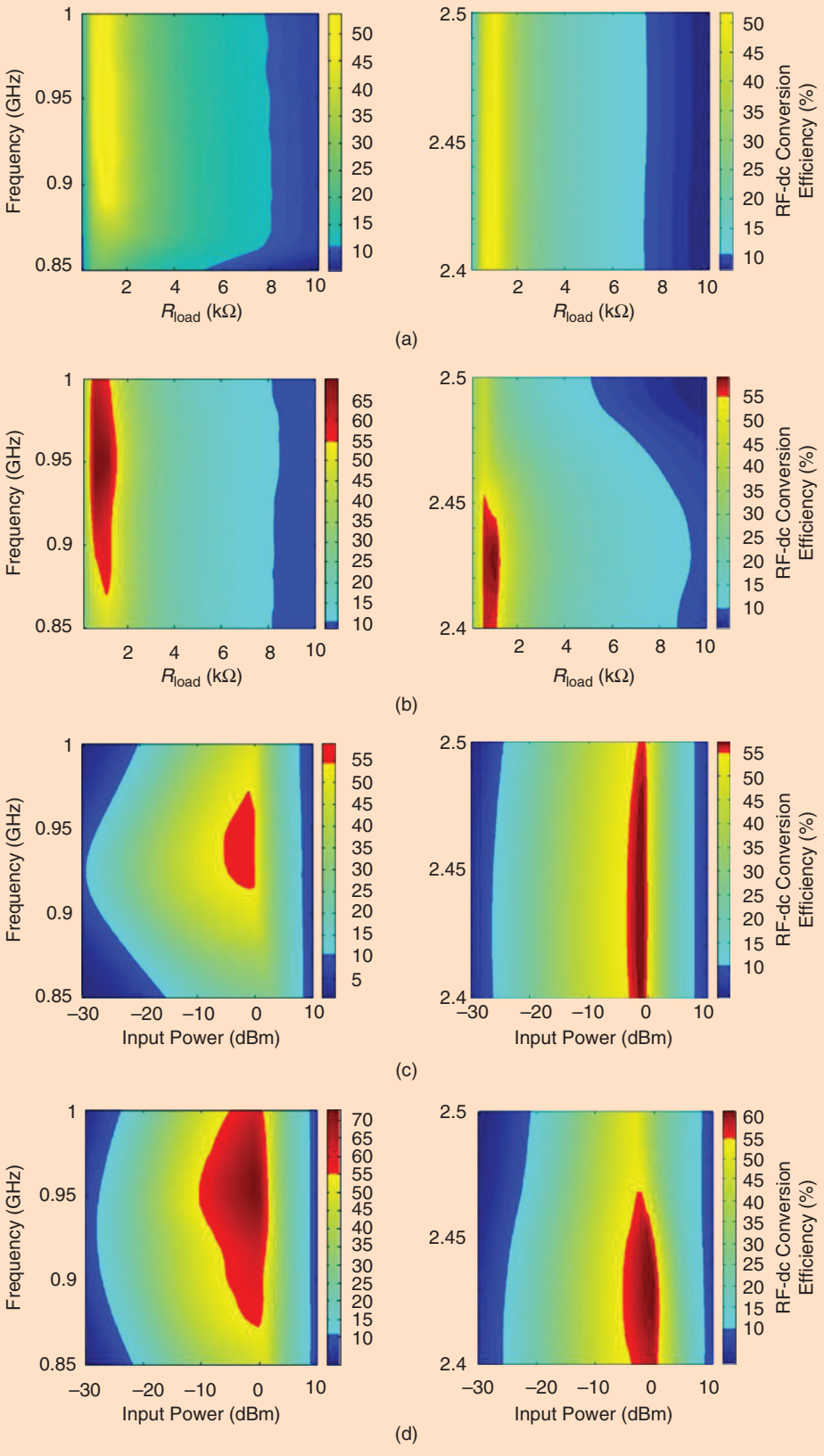

Figure 19. *RF-to-dc conversion efficiency in both frequency bands for an input power of 0 dBm of (a) a single-diode rectifier and (b) the new dual-band rectifier; RF-to-dc conversion efficiency in both frequency bands for* $R_{load} = 1$ *kΩ of (c) a single-diode rectifier and (d) the new dual-band rectifier [37].*

The RF receiver side—commonly referred as the *rectenna* (for "rectifying antenna")—must be designed to comply with multiple uncertainties.

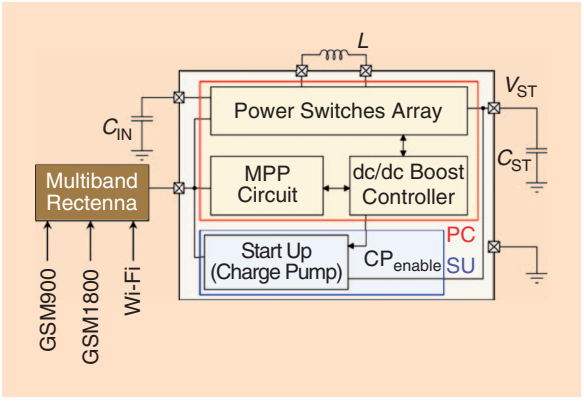

Figure 20. *A block diagram of the whole EH system deploying a triband rectenna [42].*

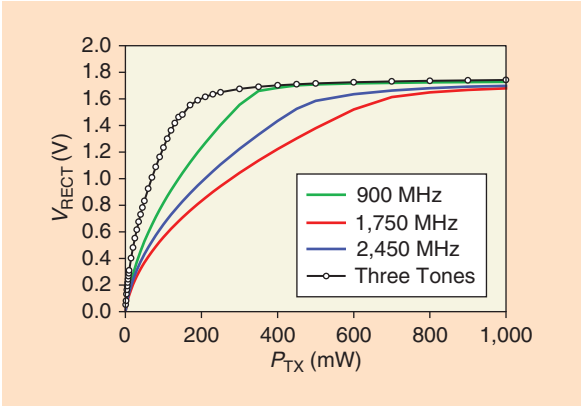

Figure 21. *The dc output voltage of a triband wearable rectenna in stationary single-tone and multitone regimes [43].*

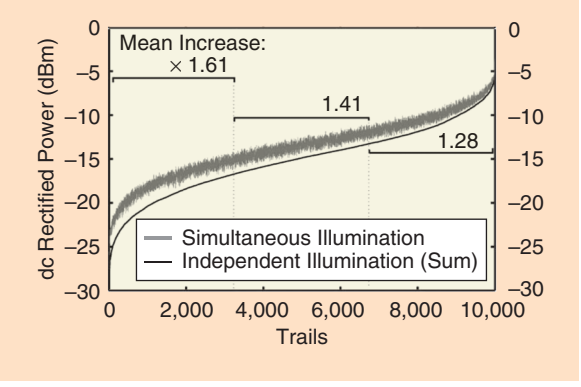

Figure 22. *A comparison of the total rectified power for independent and simultaneous dual-frequency illumination [41].*

Wideband and Multiband Rectification

The low amount of available RF power in realistic human scenarios [5]–[9] has led researchers to deploy the presence of multiple sources at different frequencies: the use of wideband or multiband antennas in EH applications is widely discussed in the literature. A multiband or multiresonant antenna can be preferable for its higher radiation efficiency because, at the resonance, the antenna provides the best radiation efficiency [38], [39]. However antennas exploiting the autosimilarity principle [40], such as Archimedean or log-periodic spiral antennas, represent a wideband solution with optimum performance [41].

The design of such a rectenna can represent a highly complex task, for the reasons already explained but also for the dispersive behavior of the antenna itself. An EM description of the antenna is mandatory for an accurate design of the whole system, but it represents an additional variable parameter to be taken into account in the design of the multifrequency matching network for a multilevel incoming signal. The solution to this problem is to design the harvester as a whole, including both the RF-to-dc converter and the PMU, as shown in Figure 20: here, the standard dc-to-dc converter (PC) for MPP tracking operation is sustained by a start-up unit (SU) for wake-up operation, in order to improve the performance of a triband wearable harvester, deploying the available wireless sources at 900, 1,800, and 2,450 MHz [42].

A multisource solution can be fruitful from another point of view: the nonlinear nature of the rectifying circuit is advantageous in the simultaneous presence of different sinusoidal (or modulated) signals because the high number of intermodulation frequency products due to the diodes' nonlinearities can be rectified as well, thus increasing the RF-to-dc conversion efficiencies. This is demonstrated by Figures 21 and 22 for a multiband [43] and a wideband rectenna [41], respectively.

Figure 21 reports the simulated rectified voltages on a fixed 900-Ω load placed at the output port of a textile triband rectenna, resulting from the superposition of different sources (the line made up of circles in the figure) and from a single source at a time, as a function of the power transmitted by a resonant half-wavelength dipole. The transmitted power values shown in the figure are associated with one excitation in the single-tone analyses and are equally distributed among the different tones in the multitone case. It is worth noting that the advantage from intermodulation distortion is significant at lower-power transmission levels, which are typical of harvesting scenarios, and becomes negligible at higher powers due to the nonlinear behavior of the diode (for the same reasons discussed in the previous section on optimized transmitted waveforms).

Figure 22 shows similar results for a log-periodic spiral antenna [41]: the comparison here is of the

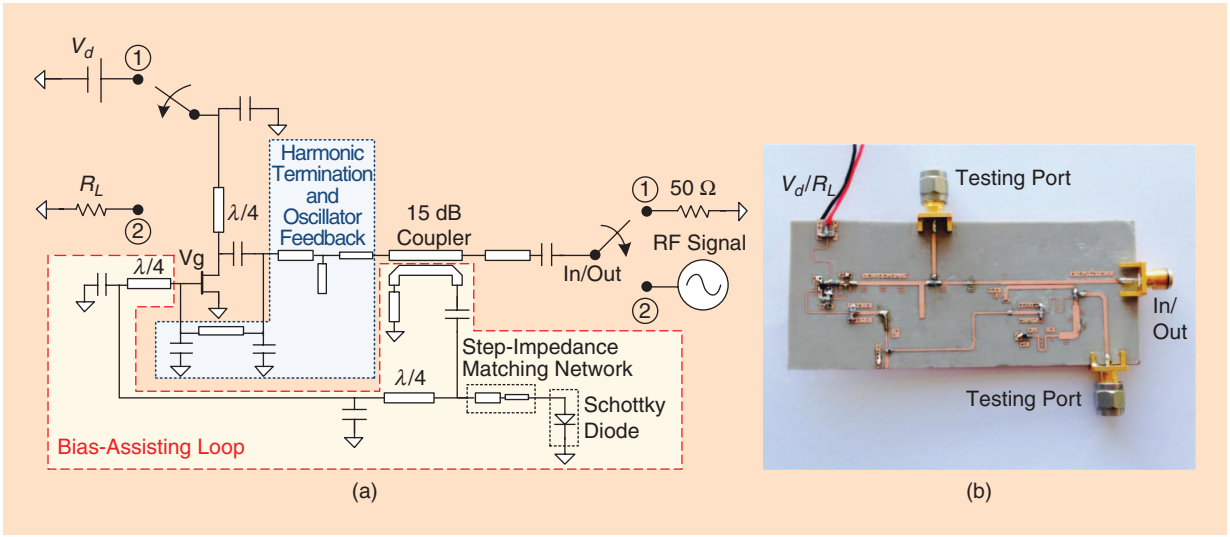

Figure 23. *An oscillator/rectifier circuit with a bias-assisting feedback loop: (a) the schematic of the circuit and (b) the fabricated prototype [47].*

total rectified power for independent and simultaneous dual-frequency illumination for 10,000 randomized input pairs of frequency sources falling in the 2–8-GHz band. The mean increase due to the contemporaneous presence of RF sources is always significant.

Bidirectional Wireless Relay Nodes

In view of a seamless reconfiguration of architectures based on wireless devices, there is great interest in devices that can integrate both RF EH and wireless power transfer capabilities, thus acting on demand either as a user or as a wireless power provider. If such devices operate bidirectionally either to exploit the harvested power themselves or to act as power relay nodes with the highest possible conversion efficiency, they can be used to provide energy to randomly but closely located wireless devices. In this way, such wireless devices can be dynamically relocated, counting on these power relay nodes. The power relay nodes thus allow the maximization of both η_{RF-RF} and η_{RF-DC} in (1), due to their bidirectional use.

A promising solution for this strategic node is presented in [44], where it is demonstrated that, for medium power transfer (on the order of a few watts), class-F RF power amplifiers exhibit comparable efficiencies when operated as self-synchronous rectifiers. In [45], this concept is extended to a 2.14-GHz, 85%-efficient 10-W class-F^{-1} rectifier. A reconfigurable class-E oscillator/rectifier in the UHF band is detailed in [46] for RF power in the microwatt range. In both operating states, high conversion efficiencies are obtained for specific gate and drain dc biases, which is a limiting factor for system operation.

In [47], a novel circuit solution is presented with bidirectional functionality and, more importantly, without the need for external batteries: it makes use of the energy stored during the rectifier's operation mode to act as a repeater. The same nonlinear circuit performs the two operations, where two switches are simultaneously driven to position 1 for oscillator operation and to position 2 for rectifier operation, as shown in Figure 23(a). The main novelties of this solution, extensively proved in [48], are 1) the implementation of self-biasing in the transistor [49] for proper oscillator class-F operation and 2) increased efficiency in the rectifier mode at low-input power levels by means of a bias-assisting feedback loop. In this way, the circuit does not need a dedicated gate bias supply, thus eliminating on-board batteries and enabling a completely energy-autonomous device with high efficiency in both the transmit and power-receive modes.

The performance of the prototype shown in Figure 23(b) is summarized in Figure 24. Figure 24(a) shows the output power and dc-to-RF conversion efficiency of the circuit operating as an oscillator as a function of drain-supply voltage. It can be observed that the efficiency remains above 50% over most of the drain-supply range. The oscillator mode has a maximum dc-to-RF conversion efficiency of 55.6% at 4.8 V drain-bias and an output power of 12 dBm. Figure 24(b) shows the measured RF-to-dc conversion efficiency in rectifying mode, as a function of input power. The plots show that the circuit is able to operate with efficiency higher than 45% starting from as low as –4 dBm of input power. This performance is preserved over a 22-dB range of input power. The circuit is able to operate even at lower input power levels but with reduced efficiency (20% efficiency for –10-dBm input power).

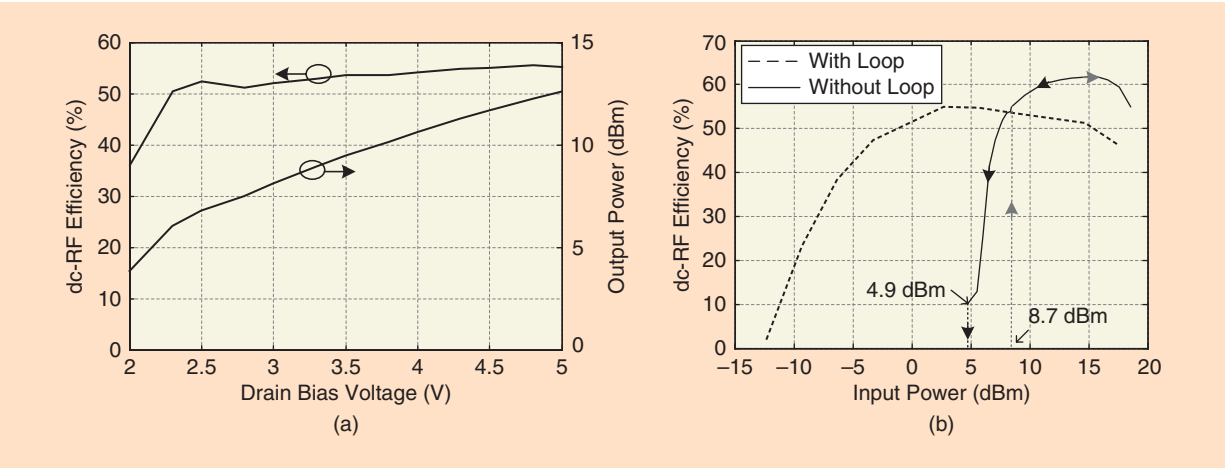

Figure 24. *(a) The measured output power and dc-to-RF efficiency of the oscillator/rectifier circuit illustrated in Figure 23, operating in oscillator mode. (b) The measured RF-to-dc conversion efficiency for the oscillator/rectifier circuit operating in rectifier mode [47].*

Conclusion

In this article, we have considered some of the most recent RF/microwave circuit and signaling solutions to assist wireless powering of maintenance-free devices and to take a step forward in the reliable implementation of cooperative smart spaces. This is currently among the most important requirements for the increasingly widespread world of pervasive monitoring, including ambient assisting living, structural monitoring, e-health, agriculture, and risk-preponderant working environments. In such scenarios, low-duty-cycle, low-power (tens of μW) wireless sensors nodes are adopted, possibly realized in eco-friendly material and without batteries.

Ambient RF EH has been successfully demonstrated to comply with these requirements, but due to its strongly environment-dependent performance and intermittent availability, it is not foreseen as a robust solution. On the other hand, dedicated RF sources providing power on demand, with optimized densities and time-interval operations, are foreseen as a more reliable choice. It has already been proven that, by a concurrent optimization of the transmitter and the receiver side, both interference and EM pollution can be kept under control. At the transmitter side, smart beaming, combined with real time localization techniques, can be coupled with optimized power waveforms to ensure, at the receiver side, successful operation of a rectifier, with input power as low as –10 dBm.

At the wireless node side, it has been demonstrated that nodes switchable between the rectifier and the power generator can autonomously operate starting at –10 dBm with an efficiency of 20% and can be exploited for providing/extracting power to/from the closely located devices, thus cooperating with the smart environment to ensure the energy autonomy balance.

References

[1] D Spenza, M. Magno, S. Basagni, L. Benini, M. Paoli, and C. Petrioli, "Beyond duty cycling: Wake-up radio with selective awakenings for long-lived wireless sensing systems," in *Proc. 2015 IEEE Conf. Computer Communications (INFOCOM)*, Apr.–May 2015, pp. 522–530.

[2] Z. Popovic, E. A. Falkenstein, D. Costinett, and R. Zane, "Low-power far-field wireless powering for wireless sensors," *Proc. IEEE*, vol. 101, no. 6, pp. 1397–1409, June 2013.

[3] A. Costanzo, M. Dionigi, D. Masotti, M. Mongiardo, G. Monti, L. Tarricone, and R. Sorrentino, "Electromagnetic energy harvesting and wireless power transmission: A unified approach," *Proc. IEEE*, vol. 102, no. 11, pp. 1692–1711, Nov. 2014.

[4] V. Rizzoli, A. Costanzo, D. Masotti, P. Spadoni, and A. Neri, "Prediction of the end-to-end performance of a microwave/RF link by means of nonlinear/electromagnetic co-simulation," *IEEE Trans. Microwave Theory Tech.*, vol. 54, no. 12, pp. 4149–4160, Dec. 2006.

[5] H. J. Visser, A. C. F. Reniers, and J. A. C. Theeuwes, "Ambient RF energy scavenging: GSM and WLAN power density measurements," in *Proc. 38th European Microwave Conf.*, Oct. 2008, pp. 721–724.

[6] M. Pinuela, P. D. Mitcheson, and S. Lucyszyn, "Ambient RF energy harvesting in urban and semi-urban environments," *IEEE Trans. Microwave Theory Tech.*, vol. 61, no. 7, pp. 2715–2726, July 2013.

[7] R. J. Vyas, B. B. Cook, Y. Kawahara, and M. M. Tentzeris, "E-WEHP: A batteryless embedded sensor-platform wirelessly powered from ambient digital-TV signals," *IEEE Trans. Microwave Theory Tech.*, vol. 61, no. 6, pp. 2491–2505, June 2013.

[8] A. N. Parks, A. P. Sample, Y. Zhao, and J. R. Smith, "A wireless sensing platform utilizing ambient RF energy," in *Proc. 2013 IEEE Topical Conf. Biomedical Wireless Techniques, Networks, and Sensing Systems (BioWireleSS)*, Jan. 2013, pp. 154–156.

[9] Z. Popovic, "Cut the cord: low-power far-field wireless powering," *IEEE Microwave Mag.*, vol. 14, no. 2, pp. 55–62, Mar.-Apr. 2013.

[10] A. Zai, L. Dongxue, S. Schafer, and Z. Popovic, "High-efficiency X-band MMIC GaN power amplifiers with supply modulation," in *Proc. 2014 IEEE MTT-S Int. Microwave Symp. (IMS)*, June 2014, pp. 1–4.

[11] Y. Kobayashi, M. Hori, H. Noji, G. Fukuda, and S. Kawasaki, "The S-band GaN-based high power amplifier and rectenna for space energy transfer applications," in *Proc. 2012 IEEE MTT-S Int. Microwave Workshop Series on Innovative Wireless Power Transmission: Technologies, Systems, and Applications (IMWS)*, May 10–11, 2012, pp. 271–274.

[12] M. Thian, A. Barakat, and V. Fusco, "High-efficiency harmonic-peaking class-EF power amplifiers with enhanced maximum operating frequency," *IEEE Trans. Microwave Theory Tech.*, vol. 63, no. 2, pp. 659–671, Feb. 2015.

[13] G. Nikandish, E. Babakrpur, and A. Medi, "A harmonic termination technique for single- and multi-band high-efficiency class-F MMIC power amplifiers," *IEEE Trans. Microwave Theory Tech.*, vol. 62, no. 5, pp. 1212–1220, May 2014.

[14] D. Masotti, A. Costanzo, M. Del Prete, and V. Rizzoli, "Time-modulation of linear arrays for real-time reconfigurable wireless power transmission," *IEEE Trans. Microwave Theory Tech.*, vol. 64, no. 2, pp. 331–342, Feb. 2016.

[15] W. H. Kummer, A. T. Villeneuve, T. S. Fong, and F. G. Terrio, "Ultra-low sidelobes from time-modulated arrays," *IEEE Trans. Antennas Propagat.*, vol. AP-11, no. 6, pp. 633–639, Nov. 1963.

[16] L. Poli, P. Rocca, G. Oliveri, and A. Massa, "Harmonic beamforming in time-modulated linear arrays through particle swarm optimization," *IEEE Trans. Antennas Propagat.*, vol. 59, no. 7, pp. 2538–2545, July 2011.

[17] S. Yang, Y. B. Gan, A. Qing, and P. K. Tan, "Design of a uniform amplitude time-modulated linear array with optimized time sequences," *IEEE Trans. Antennas Propagat.*, vol. 53, no. 7, pp. 2337–2339, July 2005.

[18] T. Takahashi, T. Mizuno, M. Sawa, T. Sasaki, T. Takahashi, and N. Shinohara, "Development of phased array for high accurate microwave power transmission," in *Proc. 2011 IEEE MTT-S Int. Microwave Workshop Series on Innovative Wireless Power Transmission: Technologies, Systems, and Applications (IMWS)*, May 2011, pp. 157–160.

[19] R. T. Iwami, A. Zamora, T. F. Chun, M. K. Watanabe, and W. A. Shiroma, "A retrodirective null-scanning array," in *2010 IEEE MTT-S Int. Microwave Symp. Dig.*, May 2010, pp. 81–84.

[20] A. Tennant and B. Chambers, "A two-element time-modulated array with direction-finding properties," *IEEE Antennas Wireless Propagat. Lett.*, vol. 6, pp. 64–65, 2007.

[21] M. Del Prete, D. Masotti, N. Arbizzani, and A. Costanzo, "Remotely identify and detect by a compact reader with mono-pulse scanning capabilities," *IEEE Trans. Microwave Theory Tech.*, vol. 61, no. 1, pp. 641–650, Jan. 2013.

[22] A. S. Boaventura and N. B. Carvalho, "Maximizing DC power in energy harvesting circuits using multisine excitation," in *2011 IEEE MTT-S Int. Microwave Symp. Dig.*, pp.1–4, June 2011.

[23] A. Boaventura, D. Belo, R. Fernandes, A. Collado, A. Georgiadis, and N. B. Carvalho, "Boosting the efficiency: Unconventional waveform design for efficient wireless power transfer," *IEEE Microwave Mag.*, vol. 16, no. 3, pp. 87–96, Apr. 2015.

[24] C. R. Valenta and G. D. Durgin, "Rectenna performance under power optimized waveform excitation," in *Proc. 2013 IEEE Int. Conf. RFID (RFID)*, Apr. 30–May 2, 2013, pp. 237–244.

[25] A. Collado and A. Georgiadis, "Optimal waveforms for efficient wireless power transmission," *IEEE Microwave Wireless Compon. Lett.*, vol. 24, no. 5, pp. 354–356, May 2014.

[26] H. Sakaki, T. Kuwahara, S. Yoshida, S. Kawasaki, and K. Nishikawa, "Analysis of rectifier RF-DC power conversion behavior with QPSK and 16 QAM input signals for WiCoPT system," in *Proc. 2014 Asia-Pacific Microwave Conf. (APMC)*, Nov. 2014, pp. 603–605.

[27] M. Kawashima, T. Nakamura, and K. Hata, "Construction of healthcare network based on proposed ECG and physical-activity sensor adopting energy-harvesting technologies," in *Proc. 2013 IEEE 15th Int. Conf. e-Health Networking, Applications Services (Healthcom)*, Oct. 2013, pp. 31–35.

[28] C. H. P. Lorenz, S. Hemour, W. Liu, A. Badel, F. Formosa, and K. Wu, "Hybrid power harvesting for increased power conversion efficiency," *IEEE Microwave Wireless Compon. Lett.*, to be published.

[29] K. Niotaki, A. Collado, A. Georgiadis, K. Sangkil, and M. M. Tentzeris, "Solar/electromagnetic energy harvesting and wireless power transmission," *Proc. IEEE*, vol. 102, no. 11, pp. 1712–1722, Nov. 2014.

[30] S. Lemey, F. Declercq, and H. Rogier, "Textile antennas as hybrid energy-harvesting platforms," *Proc. IEEE*, vol. 102, no. 11, pp. 1833–1857, Nov. 2014.

[31] A. Dolgov, R. Zane, and Z. Popovic, "Power management system for online low power RF energy harvesting optimization," *IEEE Trans. Circuits Syst. I*, vol. 7, no. 7, pp. 1802–1811, July 2010.

[32] A. Costanzo, A. Romani, D. Masotti, N. Arbizzani, and V. Rizzoli, "RF/baseband co-design of switching receivers for multiband microwave energy harvesting," *Sens. Actuators A, Phys.*, vol. 179, pp. 158–168, June 2012.

[33] J. Essel, D. Brenk, J. Heidrich, and R. Weigel, "A highly efficient UHF RFID frontend approach," in *Proc. IEEE MTT-S Int. Microwave Workshop on Wireless Sensing, Local Positioning, and RFID (IMWS 2009)*, Sept. 2009, pp. 1–4.

[34] C. H. P. Lorenz, S. Hemour, W. Li, Y. Xie, J. Gauthier, P. Fay, and K. Wu, "Overcoming the efficiency limitation of low microwave power harvesting with backward tunnel diodes," in *Proc. 2015 IEEE MTT-S Int. Microwave Symp. (IMS)*, May 2015, pp. 1–4.

[35] D. Masotti, A. Costanzo, P. Francia, M. Filippi, and A. Romani, "A load-modulated rectifier for RF micropower harvesting with start-up strategies," *IEEE Trans. Microwave Theory Tech.*, vol. 62, no. 4, pp. 994–1004, Apr. 2014.

[36] H. Yehui, O. Leitermann, D. A. Jackson, J. M. Rivas, and D. J. Perreault, "Resistance compression networks for radio-frequency power conversion," *IEEE Trans. Power Electron.*, vol. 22, no. 1, pp. 41–53, Jan. 2007.

[37] K. Niotaki, A. Georgiadis, and A. Collado, "Dual-band rectifier based on resistance compression networks," in *Proc. 2014 IEEE MTT-S Int. Microwave Symp. (IMS)*, June 1–6, 2014, pp. 1–3.

[38] D. Masotti, A. Costanzo, M. Del Prete, and V. Rizzoli, "A genetic-based design of a tetra-band high-efficiency RF energy harvesting system," *IET Microwaves Antennas Propagat.*, vol. 7, no. 15, pp. 1254–1263, 2013.

[39] V. Kuhn, C. Lahuec, F. Seguin, and C. Person, "A multi-band stacked RF energy harvester with RF-to-DC efficiency up to 84%," *IEEE Trans. Microwave Theory Tech.*, vol. 63, no. 5, pp. 1768–1778, May 2015.

[40] W. Wiesbeck, G. Adamiuk, and C. Sturm, "Basic properties and design principles of UWB antennas," *Proc. IEEE*, vol. 97, no. 2, pp. 372–385, Feb. 2009.

[41] J. A. Hagerty, F. B. Helmbrecht, W. H. McCalpin, R. Zane, and Z. B. Popovic, "Recycling ambient microwave energy with broad-band rectenna arrays," *IEEE Trans. Microwave Theory Tech.*, vol. 52, no. 3, pp. 1014–1024, Mar. 2004.

[42] M. Dini, M. Filippi, A. Costanzo, A. Romani, M. Tartagni, M. Del Prete, and D. Masotti, "A fully-autonomous integrated rf energy harvesting system for wearable applications," in *Proc. 2013 European Microwave Conf. (EuMC)*, Oct. 6–10, 2013, pp. 987–990.

[43] A. Costanzo and D. Masotti, "Wirelessly powering: An enabling technology for zero-power sensors, IoT and D2D communication," in Proc. 2015 IEEE MTT-S Int. Microwave Symp. (IMS), May 2015, pp. 1–4.

[44] T. Reveyrand, I. Ramos, and Z. Popović, "Time-reversal duality of high-efficiency RF power amplifiers," *Electron. Lett.*, vol. 48, no. 25, pp. 1607–1608, Dec. 2012.

[45] M. Roberg, T. Reveyrand, I. Ramos, E. Falkenstein, and Z. Popovic, "High-efficiency harmonically terminated diode and transistor rectifiers," *IEEE Trans. Microwave Theory Tech.*, vol. 60, pp. 4043–4052, Dec. 2012.

[46] M. N. Ruiz, A. Gonzalez, R. Marante, and J. A. Garcia, "A reconfigurable class E oscillator/rectifier based on an E-pHEMT," in *Proc. 2012 Workshop Integrated Nonlinear Microwave and Millimetre-Wave Circuits (INMMIC)*, Sept. 3–4, 2012, pp. 1–3.

[47] M. del Prete, A. Costanzo, A. Georgiadis, A. Collado, D. Masotti, and Z. Popovic, "Energy-autonomous bi-directional wireless power transmission (WPT) and energy harvesting circuit," in *Proc. 2015 IEEE MTT-S Int. Microwave Symp. (IMS)*, May 17–22, 2015, pp. 1–4.

[48] M. Del Prete, A. Costanzo, A. Georgiadis, A. Collado, D. Masotti, and Z. Popovic, "A 2.45-GHz energy-autonomous wireless power relay node," *IEEE Trans. Microwave Theory Tech.*, vol. 63, no. 12, pp. 4511–4520, Dec. 2015.

[49] H. Abe, "A GaAs MESFET self-bias mode oscillator (short paper)," *IEEE Trans. Microwave Theory Tech.*, vol. 34, no. 1, pp. 167–172, Jan. 1986.